9
Sound in Enclosures

9.1 Introduction

The behaviour of sound in volumes of air enclosed by solid boundaries is of considerable importance to noise control engineers, particularly in relation to the acoustic comfort of passengers in road, rail, air and marine vehicles. Very large amounts of money are spent by manufacturers in this regard because it is one of the major factors that influence potential purchasers. Excessive cabin noise also degrades performance and presents a health hazard for truck drivers and air crew. The enclosures of space vehicles that carry space satellites must be designed to exclude the rocket noise at launch to a degree sufficient to prevent damage to the payload. Other forms of enclosure of engineering interest include industrial work spaces, noise control enclosures for machinery and plant, machinery rooms, cavities between double walls and windows, and various forms of industrial plant, such as heat exchangers. Theoretical models of sound fields in large reverberant spaces form the basis of standardized measurement methods for the determination of source sound power, the sound transmission loss of partitions, and the diffuse field sound absorption coefficient of materials.

The acoustic behaviour of liquid-filled enclosures, such as water-cooled nuclear reactors, rocket propellant fuel tanks, flooded sonar domes, and even highly pressurized gas containers, is also of engineering interest; but the interaction between the containers and the contained liquid is so strong that vibroacoustic analysis must deal with the fully coupled problem. The analytical and behavioural complexity puts such problems outside the scope of this book.

Much of the literature on enclosure acoustics pertains to performance spaces such as concert halls and theatres. In this area of the subject, the central interests are in the relation between the physical form of the sound field and the associated psychoacoustical phenomena: speech intelligibility, quality of musical sound, the effect on performers, and the subjective response of listeners. Although these facets of the subject are fascinating, and still intensively researched, they are comprehensively covered by many specialized books on architectural acoustics (e.g. *Auditorium Acoustics and Architectural Design* (Barron, 1993) and *Room Acoustics* (Kuttruff, 2000), listed in the Bibliography) and will not feature here.

Interference between repeated reflections of sound from the boundaries of an enclosure that is not highly absorbent creates a spatially and temporally complex field that exhibits five principal features: resonance associated with acoustic modes; reverberation, in which the sound energy density decays approximately exponentially following the cessation of source activity; convoluted patterns of energy flow; a tendency to spatial uniformity of mean square pressure in response to broadband excitation; and

unpredictability. As we shall see later in this chapter, the average separation between adjacent resonance frequencies decreases as the square of frequency, so that identification of individual resonances and modes is generally impossible above about five times the fundamental resonance frequency. At sufficiently high frequency, and with a source of sufficient bandwidth, sound fields in enclosures approximate to an ideal model known as the 'diffuse field' in which every point is assumed to receive mutually uncorrelated plane waves with uniform probability of direction.

Enclosures usually contain objects of various size, and the boundaries are often geometrically irregular and formed from a variety of materials having different acoustic properties, so that incident sound waves are scattered and diffracted to form a highly complex acoustic field. Because sound waves are repeatedly reflected, even very small departures from perfect regularity and/or uniformity of boundaries are sufficient to make enclosed sound fields unpredictable at any specific location, the uncertainty increasing with frequency. This led the eminent acoustic consultant Theodore Schultz in 1973 to marvel as follows: '... it is almost incredible to me that we could produce such a complex and mysterious thing, just by putting up four walls, a floor and a ceiling, and then radiating sound into it. And yet the more we study sound in an enclosed space, the more peculiar it seems' [9.1].

The phenomenon of the enclosed sound field at frequencies at which the wavelength is much less than the average enclosure dimension is thus essentially chaotic in nature. The problem of deterministic prediction of the sound pressure at any point is akin to the problem of predicting the final rest position of a billiard (snooker, or pool) ball when struck so fiercely that it undergoes five or more rebounds. The sensitivity to the angle of the initial trajectory is quite remarkable, as successive attempts to repeat a given shot will demonstrate. Fortunately, the high density and essential uncertainty of the exact frequencies and mode shapes of high-order modes allows statistical statements to be made about the spatial probability distributions of sound pressure and sound intensity, and about the characteristics of frequency response curves. These matters are of interest for those concerned with the random error and confidence in estimates based upon sampled field data, but are best treated in specialist monographs such as *Room Acoustics* (Kuttruff, 2000) and *Sound Intensity* (Fahy, 1995) – both listed in the Bibliography, and are only briefly mentioned here.

An assumption of the existence of one particularly simple probabilistic model of a sound field, known as the diffuse field, is made in the modelling of many problems of practical concern to engineers, particularly in relation to measurement procedures; for this reason it is discussed in some detail. Because it is so widely employed, it is important to appreciate its limitations, as well as its convenience. It provides the basis for an energetic model that leads to estimates of reverberation times and the relation between space-average mean square sound pressures and the sound power injected into an enclosure by a source. It is also fundamental to an approach to the analysis of high-frequency structural vibration called statistical energy analysis (SEA), which is widely used by industry to predict noise caused by structural vibration, and to optimize structural design for the minimization of vibration and noise. Readers are referred to *Theory and Applications of Statistical Energy Analysis* (Lyon and de Jong, 1995 – see Bibliography) for an introduction to SEA.

In spite of the problem of uncertainty affecting sound fields in real enclosed volumes of complex shape, it is useful to analyse the acoustic behaviour of sound in geometrically regular enclosures because the features revealed are generic to all enclosed fields, and

thus provide a basis of qualitative understanding and the development of alternative models. It is also the case that some systems of engineering interest that incorporate enclosed fluid volumes or cavities, such as the combustion chambers of furnaces, the cavities between lightweight double walls and windows, the payload spaces of rocket launchers and the cabins of passenger vehicles, display undesirable acoustic behaviour at the resonance frequencies of certain individual low-order acoustic modes. The nature and controlling parameters of the problem can be identified by mathematical modelling and analysis, and suitable remedies applied, even though the exact frequencies and mode shapes are subject to uncertainty.

The chapter opens with an introduction to the general features of sound fields in enclosures as typified by frequency and impulse responses measured in a small reverberant room. An analysis of the modal characteristics of the sound field in a rectangular, hard-walled enclosure follows. The concept of modal density is introduced and an expression is developed on the basis of a wavenumber lattice diagram. Modal energy expressions are developed and the effect of finite boundary impedance is examined. The response of fluid in a rectangular enclosure to excitation by a harmonic point monopole leads to a modal series expression for the boundary Green's function, which is applied to the problem of sound radiation into an enclosure by a vibrating wall.

The exquisite sensitivity of high-order enclosure modes to small perturbations of the system rules out useful extension of the deterministic modal model to frequencies above about that of the tenth mode. A quantitative formula is presented for the frequency above which only a probabilistic model of enclosed sound fields is viable. The notion of randomness of an enclosed sound field, engendered by the unpredictability of modal parameters and responses, leads to the concept of a probabilistic model in which uncorrelated (statistically unrelated) plane waves propagate in all directions with uniform probability: this is the diffuse field. The assumption of 'uncorrelation' obviates the problem of wave interference and allows the total mean square pressures and intensities to be equated to the sum of that of each wave. It is shown how diffuse field relations between mean square pressure and intensity form the basis of an energetic model of enclosed sound fields. This yields simple expressions for the relation between reverberant energy decay rates and the sound absorption of the boundaries, and for the relation between source sound power and mean square sound pressure. These form the basis of standardized methods of determination of sound absorption coefficient of materials, the sound power of sources and the sound power transmission coefficients of partitions between enclosures.

The diffuse field is an appealing concept that leads to very simple expressions for quantities of concern to noise control engineers. However, the conditions necessary for its proximate establishment do not usually obtain in auditoria or in enclosures such as industrial workshops in which it is required to predict the noise levels and to specify noise control measures. Consequently, there is a need for alternative models that avoid the complexities of wave interference but are capable of representing non-diffuse, directional energy flux. Such models, which completely neglect the wave nature of sound, are based upon the concept of geometric 'ray' acoustics, in which sound energy is assumed to be transported by bundles of *straight* rays. They bear a strong resemblance to optical ray models. Various forms of assumption are made about the redistribution of energy when it encounters a boundary or an object within the enclosure. The closing section of this chapter briefly introduces the concepts and assumptions of geometric ray acoustics as applied to enclosures. For details of the methods of application and associated

computational procedures the reader is referred to reference [9.2]. Geometric acoustics also provides the basis of computational modelling of auditoria termed 'auralization', which allows a listener to experience the aural qualities of spaces at the design stage [9.3].

Ray acoustic models are widely employed for studies of sound propagation in a non-uniform atmosphere and in the ocean. The former subject is treated briefly in Chapter 12. A very thorough exposition of ray acoustics is presented in *Acoustics: An Introduction to its Physical Principles and Application* (Pierce, 1989 – see Bibliography).

9.2 Some general features of sound fields in enclosures

Figure 9.1 shows the magnitude and phase of the sound pressure frequency response with 1 Hz resolution in the range 0–500 Hz at a point on the axis of a 150 mm diameter loudspeaker in a small, reverberant, rectangular room of dimensions 2.3 m × 2.2 m × 2.5 m. The response is normalized on the cone acceleration of the loudspeaker. The reverberation time lies in the range 0.8 to 1.4 s. Figure 9.2 shows the frequency response in the range 0–5000 Hz (with 10 Hz resolution) and Fig. 9.3 shows the impulse response band-limited in the same frequency range. Figure 9.4 shows superimposed frequency responses at two points 10 cm apart. The effect of placing a 1 m square plywood panel in one corner of the room is shown in Fig. 9.5. The peaks in Fig. 9.1(a) indicate individual resonance frequencies of the room, of which the lowest at about 68.6 Hz corresponds to a wavelength of 5.0 m at a temperature of 20°C. The phase plot in Fig. 9.1(b) exhibits the rapid slewing of phase in the region of the resonance peaks that is characteristic of modal resonance. Above about 400 Hz, the resonance peaks begin to overlap. Above 500 Hz, no individual resonances can be detected and the phase variation bears no apparent systematic relation to the magnitude. The variation of (wrapped) phase with frequency,

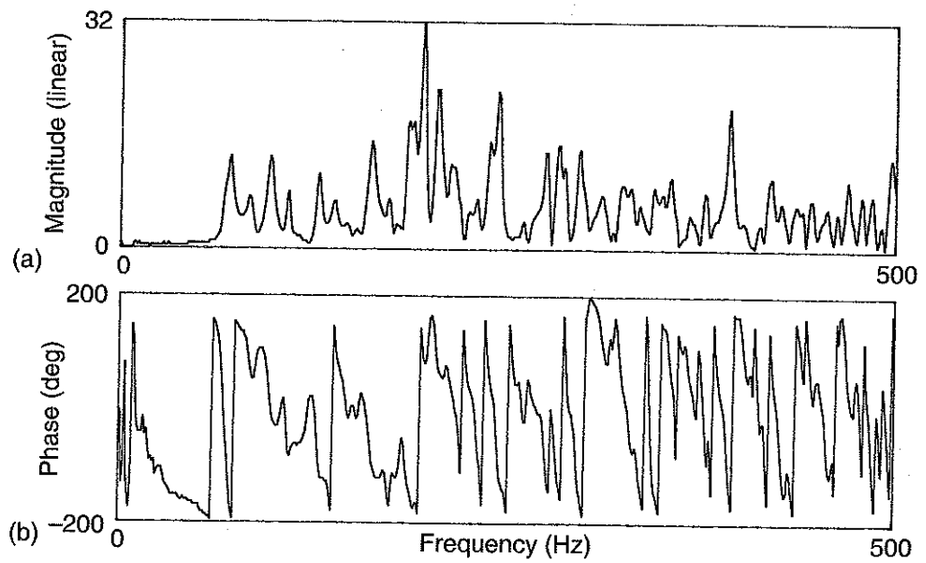

Fig. 9.1 Frequency response of a small room, 0–500 Hz: (a) magnitude; (b) phase.

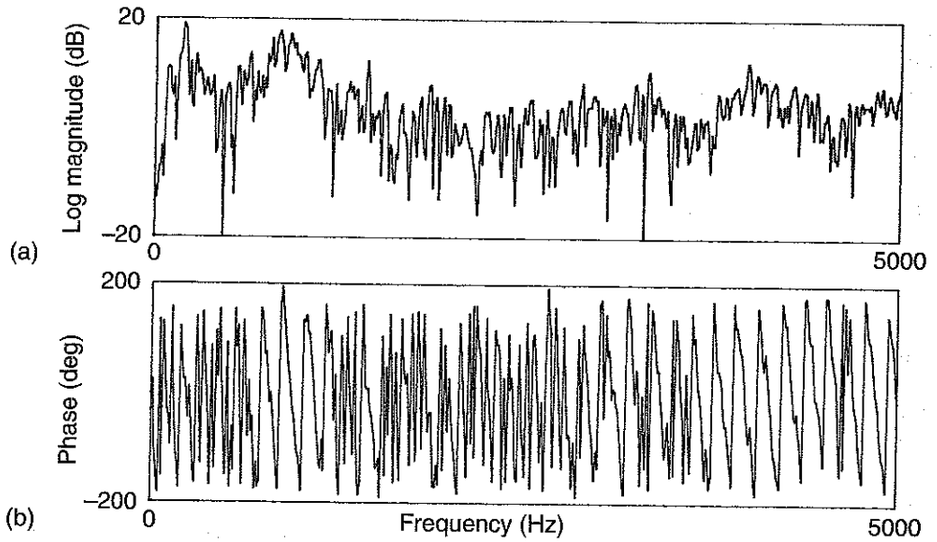

Fig. 9.2 Frequency response of a small room, 0–5 kHz: (a) log magnitude; (b) phase.

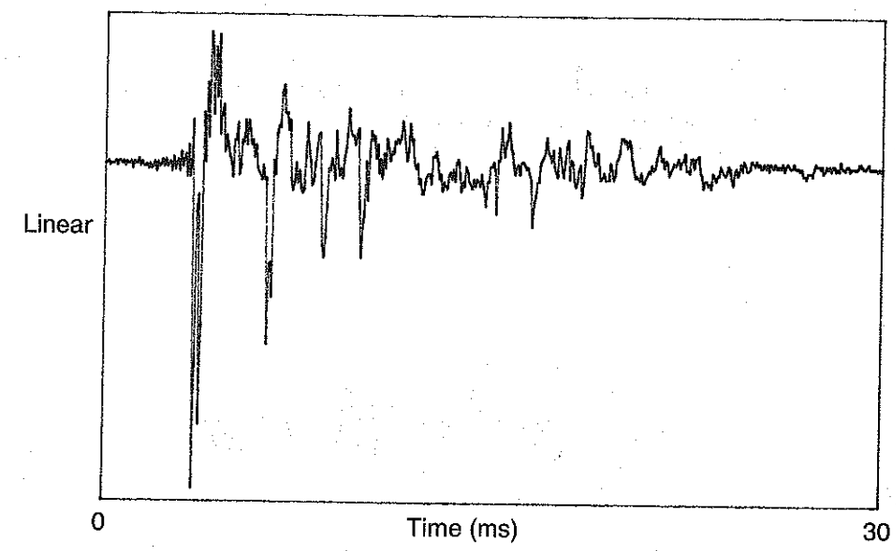

Fig. 9.3 Impulse response corresponding to Fig. 9.2.

shown in Fig. 9.2(b), reveals an underlying sawtooth pattern that corresponds to the direct field, on which is superimposed an irregular deviation caused by reverberant reflection.

The impulse response in Fig. 9.3 is the inverse Fourier transform of the frequency response in the frequency range 0–5000 Hz (see Appendix 2). The arrivals of the direct sound and the subsequent early reflections can clearly be seen. The 10 Hz bandwidth of

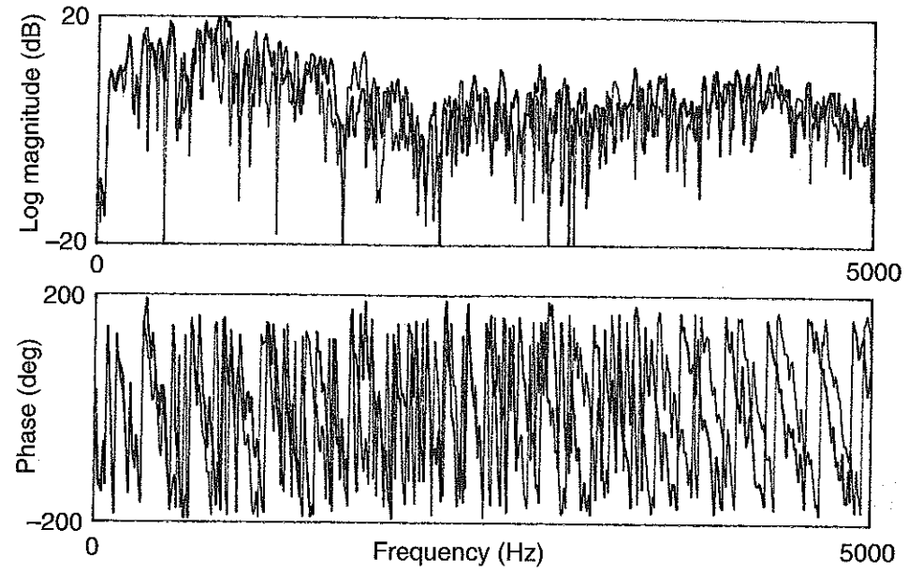

Fig. 9.4 Frequency responses measured 100 mm apart, 0–5 kHz.

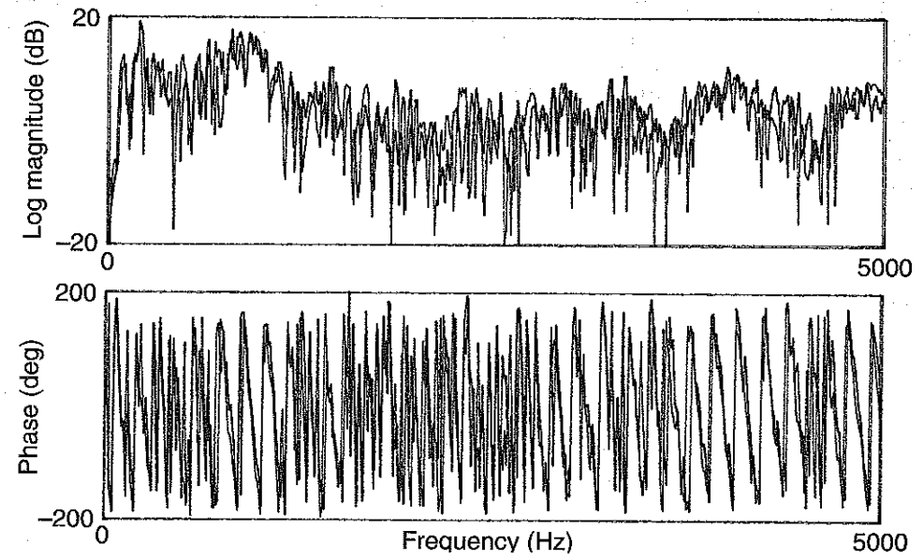

Fig. 9.5 Effect of the introduction of a 1 m^2 board on the frequency response, 0–5 kHz.

the effective filter imposed by the Fast Fourier Transform (FFT) analyser used to produce these results is wide enough to ensure that the impulse response of the filter is sufficiently short not to distort the room impulse response to an unacceptable degree. This is an example of the fundamental law of signal analysis that the product of the frequency and time resolution is constant; for a high degree of resolution in one domain

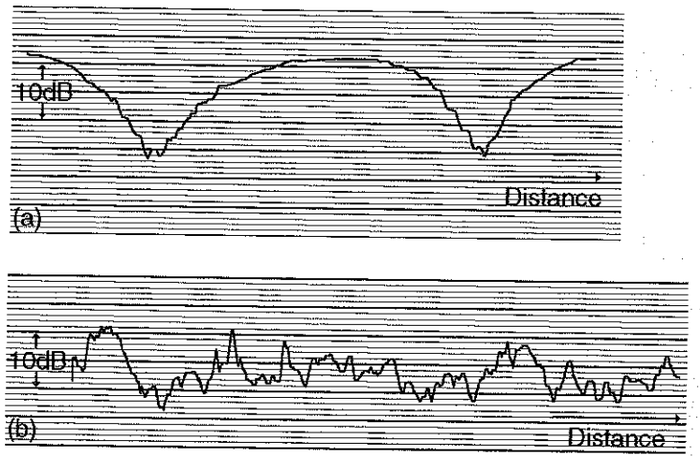

Fig. 9.6 Spatial variation of sound pressure level at an individual frequency: (a) 250 Hz; (b) 5000 Hz.

one must sacrifice resolution in the other. It is not useful to display the band-limited impulse response in the frequency range 0–500 Hz because the impulse response of the room is distorted by that of the 1 Hz narrow-band filter through a process termed 'convolution'. The filter 'rings' for a duration that is long compared with the separation in time of the individual reflections.

Figure 9.6 shows the variation of sound pressure level with position at two individual frequencies of 250 and 5000 Hz. There is similarity of ranges between the frequency response curve at a fixed point and the spatial variation of sound pressure level with position at a fixed frequency. This is a fundamental characteristic of sound fields in reverberant enclosures. Figure 9.7 shows the spatial variation of broadband sound pressure level in the 1/3 octave bands centred on 250 and 5000 Hz, which have bandwidths of about 66 and 1250 Hz. The 'smoothing' effect associated with the simultaneous excitation of a large number of modes is clearly seen at the higher frequency.

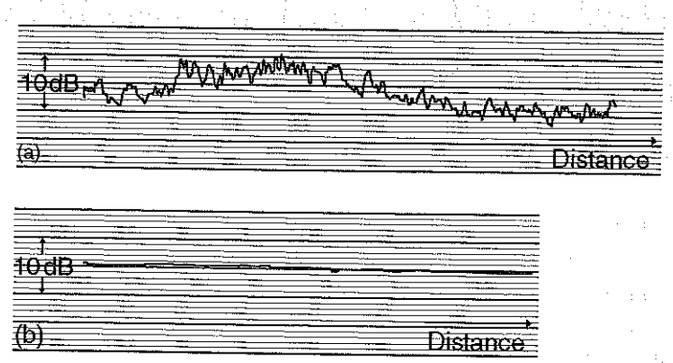

Fig. 9.7 Spatial variation of sound pressure level in a 1/3 octave band centred on: (a) 250 Hz; (b) 5000 Hz.

9.3 Apology for the rectangular enclosure

The sound field generated in any enclosed volume of fluid by a given source distribution acting within the volume and/or vibration of the boundaries, may, in principle, be determined by solving the wave equation subject to the appropriate boundary conditions. The Kirchhoff–Helmholtz integral equation derived in Chapter 6 applies. Solutions in terms of modes represented by simple analytic functions of space, such as sines, cosines, and Bessel functions, are available only for regular enclosure geometries, such as rectangular or cylindrical. More complex, irregular geometries of variable boundary impedance demand the application of discretized models and computational procedures such as the finite element and boundary element methods. These are comprehensively explained in such books as *Introduction to Finite Element Vibration Analysis* (Petyt, 1998) and *Boundary Elements in Acoustics* (Von Estorff, 2000), both listed in the Bibliography, and in the manuals of FEM and BEM software.

In this textbook, which addresses fundamentals, and aims principally to instruct in concepts, principles and phenomena, rather than engineering methods, only enclosures of rectangular geometry will be studied. The physical behaviour revealed is common to all enclosures; only the temporal and spatial complexity of the fields vary.

9.4 The impulse response of fluid in a reverberant rectangular enclosure

In the preceding chapter, a study of the behaviour of waves generated in a tube by an impulsively displaced piston led to the identification of acoustic natural frequencies associated with periodicity of arrivals of reflections. In principle, it is possible in a similar manner to determine the natural frequencies of the standing wave modes of a three-dimensional rigid-walled rectangular enclosure by exciting it by an impulsive point monopole source and following the passage of the resulting spherical wavefront as it makes successive encounters with the enclosure boundaries. Each reflection may be represented by the wavefront generated by an identical (virtual) source located at an image point (as if the real source 'saw' itself in a gallery of plane mirrors placed on the enclosure boundaries). In practice, it is only straightforward to identify the natural frequencies of a small subset of all possible modes because a comprehensive analysis requires examination of the geometrical properties of an infinite set of images – a not inconsiderable task.

However, the source image diagram does provide a useful means of visualizing the arrival sequence and relative strengths of reflections of sound generated by an impulsive point monopole, and it can be adapted to handle source directivity. A three-dimensional image source array is difficult to represent and interpret on paper, so a two-dimensional enclosure is presented in Fig. 9.8. The source and its images take the form of thin, impulsively expanding, tubes that extend to infinity in both directions normal to the plane of the paper. If the enclosure walls are perfectly reflective, all the images are identical to the physical source and are *simultaneously activated*. The distance travelled by each circular wavefront in time t is $r = ct$. The sound pressure of each circular cylindrical pulse wave varies as $r^{-1/2}$ (unlike spherically spreading wavefronts). The average rate of arrival of reflections at elapsed time t may be approximately estimated by dividing the area of the annulus of radius $r = ct$ and width $\Delta r = c\Delta t$ by ab, which is the

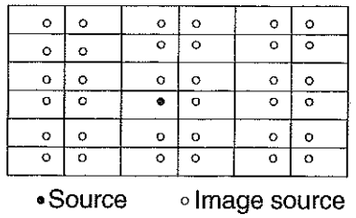

Fig. 9.8 Two-dimensional image array.

area occupied by each image source. Approximately $2\pi c^2 t\,\Delta t/S$ reflections arrive in time Δt, giving an asymptotic rate of arrival of $2\pi c^2 t/S$, where S is the area of the enclosure. Consideration of the equivalent three-dimensional diagram shows that the asymptotic rate of arrival is $4\pi c^3 t^2/V$, where V is the enclosure volume.

In a perfectly reflective enclosure, progressively weaker reflections continue to arrive at progressively increasing rates for an infinite time. Energy conservation is satisfied because the product of the pulse arrival rate and intensity produced by an individual image source is independent of time. If the enclosure walls are plane, but have a non-zero, locally reactive, impedance, spherical incident wavefronts *do not result in spherical reflected wavefronts*. This may be qualitatively explained by the fact that the angle of intersection of a spherical wavefront with a plane surface varies with position on the wavefront. (The problem may be rigorously analysed by mathematically decomposing a spherical wavefront into an infinity of plane waves in a manner similar to spatial Fourier analysis; see *Waves in Layered Media* (Brekhovskikh, 1960), listed in the Bibliography.) However, as a reasonable approximation for enclosures whose walls have a diffuse field absorption coefficient α_d much less than unity, so that the field remains reverberant, one may factor the image strength by α_d on the basis that each wall receives incident waves from all directions with equal probability, because the rate of decay of sound energy is slow compared with the rate of arrival of reflections. The rate of arrival of energy in the enclosure decreases with time, and the sound field decays.

The image model constitutes a useful device for understanding the distinction between the meanings of the terms 'reverberant' and 'diffuse' as applied to sound fields in enclosures, which is often blurred in the literature. The sound field in a long, concrete-walled, uncarpeted corridor is reverberant, because the proportion of stored energy lost per reflection is very small. However, reference to the source image diagram for such a long, thin space clearly shows that the distribution of directions of reflection arrival is far from uniform. The field is therefore nowhere near diffuse. The contrary case is not common, but could be established at the centre of an array of uncorrelated point sources distributed uniformly over a spherical surface in free field. This is approximated by certain standardized tests for ear defender performance.

However, the asymptotic statistical estimate of average rate of arrival of pulse reflections at a receiver point does not apply to the first few 'early' reflections. These crucially influence the intelligibility of speech and the clarity of musical sound in auditoria. Consequently, theoretical and experimental studies of the time and strength of arrival, together with direction of arrival, form a key element in the prediction and evaluation of the quality of auditorium performance. Details will be found in publications specifically dedicated to this subject, such as *Room Acoustics* (Kuttruff, 2000 – see Bibliography).

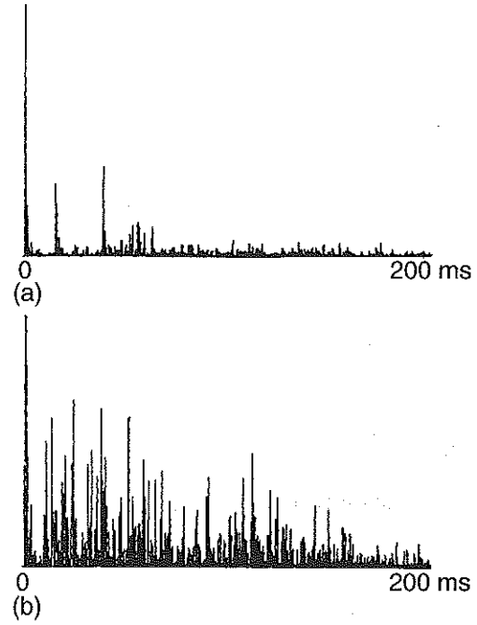

Fig. 9.9 Pressure-squared impulse responses in the Royal Festival Hall, London: (a) 18 m from the source; (b) 35 m from the source. Reproduced with permission from Barron, M. (1993) *Auditorium Acoustics and Architectural Design*. E & F N Spon, London.

In practice, the boundaries of all enclosures scatter a greater or smaller proportion of incident energy into non-specular directions, thus severely limiting the usefulness of the image model for predictive purposes. An example of the actual pressure-squared impulse response, or misleadingly called 'echogram', of a large auditorium is shown in Fig. 9.9. The densely populated tail is defined as 'reverberation'. Reflections arriving within about 50 ms of the direct sound are not subjectively perceived as 'echoes'.

9.5 Acoustic natural frequencies and modes of fluid in a rigid-walled rectangular enclosure

The rectangular enclosure shown in Fig. 9.10 may be considered as a section of duct of rectangular cross-section closed by two plane surfaces oriented at right angles to the duct axis. Consequently, solutions to the homogeneous Helmholtz equation, subject to the boundary conditions of zero normal pressure gradient, are readily obtained by requiring the sum of the two modal solutions of Eq. (8.81) to meet this condition at $z = 0$ and $z = c$. The resulting expression for modal pressure distribution is

$$p_{lmn}(x, y, z) = A_{lmn} \cos(l\pi x/a) \cos(m\pi y/b) \cos(n\pi z/c) \tag{9.1}$$

in which the notation of the mode order indices has been altered from that in Eq. (8.81) to make it more logically related to the coordinate system. The corresponding expressions relating modal wavenumber and natural frequency to the component

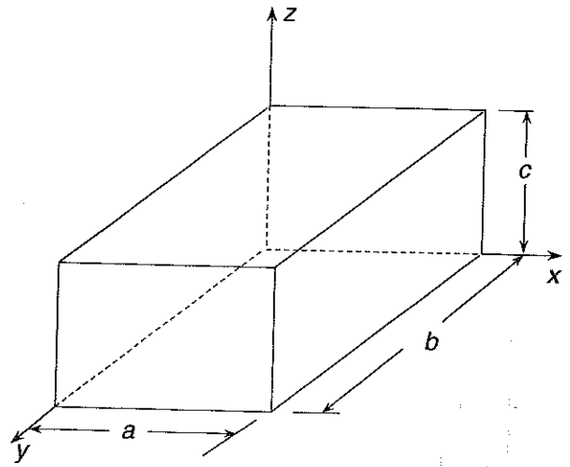

Fig. 9.10 Rectangular enclosure.

wavenumbers are

$$k_{lmn}^2 = (l\pi/a)^2 + (m\pi/b)^2 + (n\pi/c)^2 \tag{9.2a}$$

and

$$\omega_{lmn}^2 = c^2 k_{lmn}^2 \tag{9.2b}$$

The relation expressed by Eq. (9.2a) is conveniently visualized by means of the wavenumber lattice diagram shown in Fig. 9.11. Each mode is represented by an intersection of the grid lines (lattice point). Lattice points lying on each of the three axes represent 'axial' modes in which the field quantities are uniform over planes normal to the relevant axis. Lattice points lying in the x–y, x–z and y–z planes represent 'tangential' modes, in which the field quantities are uniform in z, y and x directions, respectively. All other modes are termed 'oblique'. Each modal standing wave

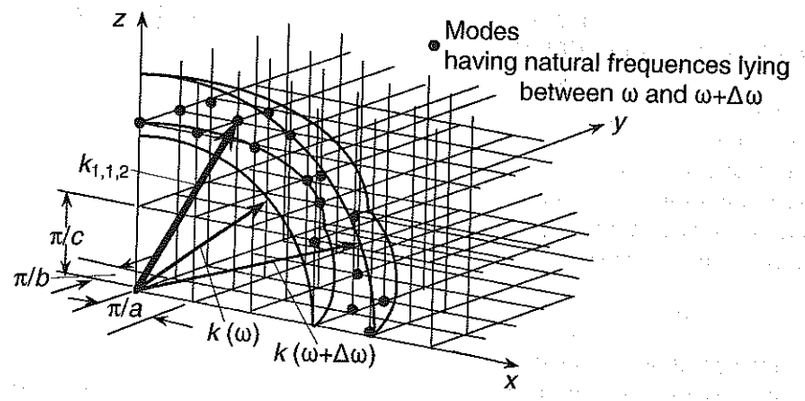

Fig. 9.11 Wavenumber lattice with superimposed frequency band shell.

(eigenfunction) may be decomposed into two (axial), four (tangential) or six (oblique) oppositely directed plane travelling waves of equal amplitude. Two examples follow.

Axial: $A \cos(l\pi x/a) \exp(j\omega t) = \frac{1}{2}A \exp[j(\omega t - l\pi x/a)] + \frac{1}{2}A \exp[j(\omega t + l\pi x/a)]$ (9.3a)

Tangential: $B \cos(l\pi x/a) \cos(m\pi y/b) \exp(j\omega t)$
$= \frac{1}{4}B \exp[j(\omega t - l\pi x/a - m\pi y/b)] + \frac{1}{4}B \exp[j(\omega t - l\pi x/a + m\pi y/b)]$
$+ \frac{1}{4}B \exp[j(\omega t + l\pi x/a - m\pi y/b)] + \frac{1}{4}B \exp[j(\omega t + l\pi x/a + m\pi y/b)]$ (9.3b)

The modal wavenumber vector, which joins the coordinate origin to the modal lattice point, together with its reflection in the x–y, x–z and y–z planes, as appropriate, indicate the direction of propagation of these travelling plane wave components.

The wavenumber lattice construction provides a convenient means of estimating the distribution of modal natural frequencies as a function of frequency. It is also extremely useful in studies of acoustic coupling between enclosed fluids and the flexible walls of an enclosure, as we shall see later. The actual distribution of acoustic natural frequencies of a rectangular enclosure is not a smooth function of frequency, as evidenced by the example of cumulative mode count illustrated by Fig. 9.12. However, a smoothed estimate of the *density* of the distribution is obtained by noting that each mode point occupies a volume of wavenumber 'space' equal to π^3/abc. The locus of constant acoustic wavenumber k (or $\omega = ck$) lies on the spherical surface as shown in Fig. 9.11. This surface encloses a volume of wavenumber space equal to $\pi k^3/6$ in one octant. Hence, the number of modes having natural frequencies lying below ω is given approximately by

$$N(\omega) \approx \omega^3 abc/6\pi^2 c^3 = \omega^3 V/6\pi^2 c^3 \tag{9.4}$$

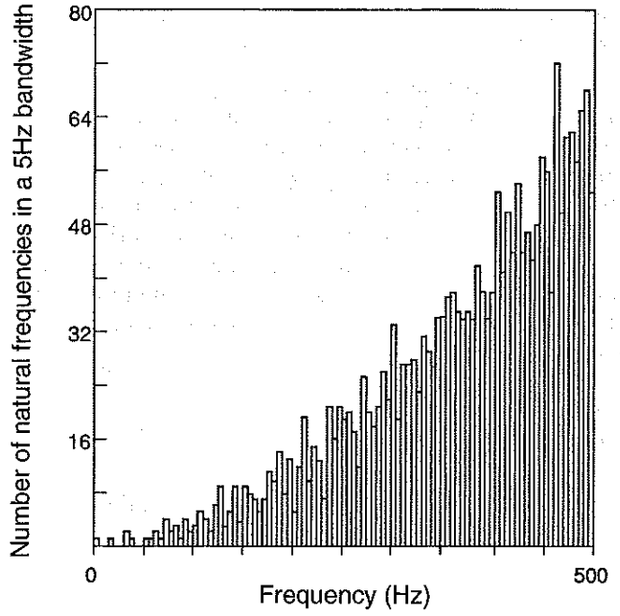

Fig. 9.12 Cumulative mode count of a 10 m × 5 m × 3 m enclosure. Reproduced with permission from Nelson, P. A. and Elliott, S. J. (1992) *Active Control of Sound*. Academic Press, London.

where $V = abc$. The average number of modal natural frequencies per unit frequency is given approximately by

$$\partial N/\partial\omega \approx \omega^2 V/2\pi^2 c^3 \tag{9.5a}$$

In terms of frequency f (Hz)

$$\partial N/df \approx 4\pi f^2 V/c^3 \tag{9.5b}$$

A more accurate expression may be obtained by making individual estimates of the density of axial, tangential and oblique modes. The results are as follows:

$$\partial N_a/\partial f = L/2c \tag{9.6a}$$

$$\partial N_t/\partial f = \pi Sf/c^2 - L/2c \tag{9.6b}$$

and

$$\partial N_o/\partial f = 4\pi f^2 V/c^3 - \pi Sf/2c^2 \tag{9.6c}$$

where $S = 2(ab + bc + ac)$ and $L = 4(a + b + c)$.

The relative densities of the three classes of mode depend upon the relative dimensions of the enclosure. As frequency rises, the modal density becomes increasingly dominated by that of the oblique modes, and the expression in Eq. (9.5) is known as the 'asymptotic modal density'. It has been shown by statistical analysis, the details of which need not concern us, that this expression applies in the asymptotic limit to any single space enclosure, of whatever geometric form. The three expressions of Eq. (9.6) should be separately evaluated in cases of highly disproportionate enclosures, such as long corridors or large rooms with low ceilings.

Example: The asymptotic modal density of the very small room described in Section 9.2 is 0.16 modes Hz^{-1} at 200 Hz and 4 modes Hz^{-1} at 1 kHz.

There exists a rather widely held view that standing waves and modal resonances can be weakened, or even eliminated, by making the boundaries of reverberant enclosure non-parallel or geometrically irregular. This view is erroneous. Reverberant enclosures of all shapes exhibit these features. The only way to suppress the interference effects that underlie such behaviour is to introduce sufficient absorption into the enclosure to eliminate multiple reflection. It is true, however, that the distribution of modal natural frequencies and mode shapes can be altered by modification of enclosure geometry. Certain ratios of rectangular room dimensions produce more uniform distribution of modal natural frequencies than others and are therefore favoured for small enclosures such as recording or broadcasting studios.

9.6 Modal energy

The time-average kinetic and potential energy densities of a time-stationary sound field are given by the time averages of Eqs (5.4) and (5.5)

$$\overline{e_k} = \tfrac{1}{2}\rho_0(\overline{u^2} + \overline{v^2} + \overline{w^2}) \tag{9.7a}$$

in which u, v and w are the Cartesian components of the particle velocity vector **u**, and

$$\overline{e_p} = \tfrac{1}{2}\overline{p^2}/\rho_0 c^2 \tag{9.7b}$$

We assume an isolated acoustic mode in a rigid-walled, rectangular enclosure to be oscillating harmonically with frequency ω. The pressure field takes the form

$$p(x, y, z, t) = \tilde{A}_N \cos(l\pi x/a) \cos(m\pi y/b) \cos(n\pi z/c) \exp(j\omega t) \tag{9.8}$$

where the subscript N stands for lmn.

The time-average potential energy density at point (x, y, z) is given by

$$\overline{e_p}(x, y, z) = (|\tilde{A}_N|^2/4\rho_0 c^2) \cos^2(l\pi x/a) \cos^2(m\pi y/b) \cos^2(n\pi z/c) \tag{9.9}$$

The total time-average potential energy is given by the integral of this expression over the volume of the enclosure as

$$\overline{E_p} = |\tilde{A}_N|^2(abc)/32\rho_0 c^2 \tag{9.10}$$

in which a is replaced by $2a$ when $l = 0$, b is replaced by $2b$ when $m = 0$ and c is replaced by $2c$ when $n = 0$. This is the 'null index' convention, which will be used extensively in this chapter.

The components of modal particle velocity are given by Eqs (3.34) as

$$u = -j(1/\omega\rho_0)(l\pi/a)[\tan(l\pi x/a)]p \tag{9.11a}$$

$$v = -j(1/\omega\rho_0)(m\pi/b)[\tan(m\pi y/b)]p \tag{9.11b}$$

$$w = -j(1/\omega\rho_0)(n\pi/c)[\tan(n\pi z/c)]p \tag{9.11c}$$

The time-average kinetic energy density is

$$\overline{\varepsilon_k} = (1/2\omega^2\rho_0)[(l\pi/a)^2 \tan^2(l\pi xa) + (m\pi/b)^2 \tan^2(m\pi y/b) + (n\pi/c)^2 \tan^2(n\pi z/c)]\overline{p^2} \tag{9.12}$$

which, when integrated over the enclosure volume, yields

$$\overline{E_k} = |\tilde{A}_N|^2(abc)k_{lmn}^2/32\rho_0\omega^2 \tag{9.13}$$

subject to the same convention with regard to null modal indices as before.

The time-average potential and kinetic energies are equal only if the mode oscillates at its natural frequency given by Eq. (9.2b), or is excited by broadband noise.

9.7 The effects of finite wall impedance on modal energy–time dependence in free vibration

The boundaries of all physical enclosures vibrate in response to incident sound and are to some extent sound absorptive. We have seen in Chapter 8 that the natural frequencies of acoustic modes of fluid in tubes having terminations of finite reactive impedance are altered from those with a rigid termination. We have also seen that the presence of a resistive component of termination impedance renders the natural modes complex in wavenumber and natural frequency. Extension of the analysis of the sound field in a two- or three-dimensional enclosure with walls of arbitrary impedance is possible, but the resulting expressions are complex and quantitative solutions require the application of iterative numerical analysis (see reference [9.4]). Alternatively, variational techniques may be applied in the form of finite element or boundary element routines.

A completely general treatment of free vibration is therefore well beyond the scope of

this text. However, provided that the magnitude of specific acoustic impedance ratio of the boundaries is very much greater than unity, as it is, for example, in reverberation chambers and unfurnished rooms, little error is made by assuming that the modes closely approximate rigid-wall modes, each vibrating at a complex frequency of which the real part equals its rigid-wall value. Because the ratio of imaginary to real part is very small, the fractional decrease of modal amplitude per cycle of free oscillation is so small that quasi-steady conditions may be assumed to obtain. As suggested by the analysis in Section 8.4.2, we may then neglect mode coupling at the boundaries. Hence, on the basis of the assumption of local reaction, the time-average rate of absorption of modal sound energy per unit area of boundary may be approximated by

$$\tfrac{1}{2}(\overline{p_{Nb}^2}/\rho_0 c)\ \mathrm{Re}\ \{1/z_n'\} \tag{9.14}$$

where p_{Nb} is the modal pressure at a boundary having specific acoustic impedance ratio z_n'. When integrated over a period of time that encompasses a number of cycles of the lowest frequency mode contributing significantly to p_b, the cross terms which express the work done by the pressure in one mode collaborating with the normal boundary velocity generated by the pressure in another mode tend to become very small compared with the 'self' or 'direct terms', which involve the pressure of one mode and the associated boundary velocity. This effect is enhanced if the modal frequencies are well separated. This model, which is valid only for rather stiff/massive walls with low absorption coefficient, indicates that absorbers are most effective if placed at pressure anti-nodes: for example in the enclosure corners.

Let us now assume that all boundaries have the same uniform impedance. (This assumption may be relaxed if appropriate.) The total rate of change of modal energy is given by the integral of the above expression over the whole boundary. Using Eq. (9.8) in Eq. (9.14) gives:

$$\mathrm{d}E_N/\mathrm{d}t = -(\tfrac{1}{4}|\tilde{A}_N|^2/\rho_0 c)\ \mathrm{Re}\ \{1/z_n'\}[ab + bc + ac] \tag{9.15}$$

to which the convention regarding null modal indices applies. Under the assumed conditions, the energy of each mode decreases at a rate that is independent of the presence of the other modes; we may therefore concentrate on individual modes. The rate of loss of modal energy is proportional to that energy, so it decays exponentially as $\exp(-\delta_N t)$, where the decay factor is given by

$$\delta_N = (\mathrm{d}E_N/\mathrm{d}t)/E_N = 4c\ \mathrm{Re}\ \{1/z_n'\}\left[\frac{1}{a} + \frac{1}{b} + \frac{1}{c}\right] \tag{9.16a}$$

which, taking into account the null index factor, is greatest for oblique modes and least for axial modes. The corresponding modal 'reverberation time' T_N, which is defined as the time for the modal energy to decay by a factor of 10^6, is

$$T_N = 6/\delta_N \log_{10} \mathrm{e} = 13{\cdot}8/\delta_N \tag{9.16b}$$

The equivalent modal loss factor (see Appendix 5) is equal to $13.8/T_N\,\omega_{lmn}$.

The variation of total energy with time is indeterminate unless the numbers and types of contributing modes are specified, together with their initial energies; these depend upon the directivity, location and frequency spectrum of the energizing source. If a measure of the decay of squared pressure at one point is used to indicate total energy decay rates, the indication will also vary with these factors. This is the reason why reverberation time measurements made using impulsive sources, such as starting pistols,

and those made after the cessation of loudspeaker excitation are likely to differ, especially if no spatial averaging procedure is employed.

The approximations and results of the above analysis are not valid if the modal density and boundary absorption are so high that individual modal resonant responses overlap and resonance peaks are not individually discernible in a frequency response curve. In such cases, the rigid-wall modes become significantly coupled and an alternative model is required. We shall return to this matter in due course.

9.8 The response of fluid in a rectangular enclosure to harmonic excitation by a point monopole source

The following analysis is an extension into three dimensions of that presented in Section 8.4.2, in which a Green's function was expressed in terms of an infinite series of rigid-wall eigenfunctions, and the K–H integral was applied to account both for the active piston source and the passive motion of the finite impedance boundaries in response to local pressure.

We shall first consider the case of arbitrary enclosure geometry and denote the rigid-wall eigenfunctions by $\psi_N(\mathbf{x})$ in which the position vector $\mathbf{x}$ stands for (x, y, z). (Remember, these are not the *natural* mode shapes of an enclosure with finite impedance boundaries.) The specific acoustic impedance ratio of the boundaries is denoted by $z_n'(\mathbf{x}_s)$, where $\mathbf{x}_s$ refers to locations on the boundary. A Green's function that satisfies the rigid-wall conditions may be expressed as an infinite series of these functions as $G(\mathbf{x}|\mathbf{x}_0) = \sum_N \tilde{A}_N \psi_N(\mathbf{x})$. According to the definition expressed in Section 6.4.2, G satisfies $\nabla^2 G + k^2 G = -\delta(\mathbf{x} - \mathbf{x}_0)$. Therefore,

$$\sum_N \tilde{A}_N \nabla^2 \psi_N(\mathbf{x}) + k^2 \sum_N \tilde{A}_N \psi_N(\mathbf{x}) = -\delta(\mathbf{x} - \mathbf{x}_0) \tag{9.17}$$

The rigid-wall eigenfunctions satisfy the homogeneous Helmholtz equation at the rigid-wall mode natural frequencies $\omega_N = ck_N$:

$$\nabla^2 \psi_N(\mathbf{x}) + k_N^2 \psi_N(\mathbf{x}) = 0 \tag{9.18}$$

Thus

$$-\sum_N \tilde{A}_N k_N^2 \psi_N(\mathbf{x}) + k^2 \sum_N \tilde{A}_N \psi_N(\mathbf{x}) = -\delta(\mathbf{x} - \mathbf{x}_0) \tag{9.19}$$

Multiplication of Eq. (9.19) by ψ_M, followed by integration over the enclosure volume V yields, by virtue of orthogonality (all terms zero except for $M = N$),

$$-\tilde{A}_N k_N^2 \Lambda_N + k^2 \tilde{A}_N \Lambda_N = -\psi_N(\mathbf{x}_0) \tag{9.20}$$

where $\Lambda_N = \int_V \psi_N^2(\mathbf{x})\,\mathrm{d}\mathbf{x}$. Hence,

$$G = \sum_N \frac{\psi_N(\mathbf{x}_0)\psi_N(\mathbf{x})}{\Lambda_N(k_N^2 - k^2)} \tag{9.21}$$

The harmonic form of the K–H equation (6.48) expresses the sound pressure at location $\mathbf{x}$ generated by a volume velocity $q(\mathbf{x}_0)$ of monopole source strength, together

with a distribution of boundary sources. $\partial G/\partial n = 0$ for the rigid-wall eigenfunctions.

$$\tilde{p}(\mathbf{x}) = j\omega\rho_0 \int_V \tilde{q}(\mathbf{x}_0) G(\mathbf{x}|\mathbf{x}_0)\, \mathrm{d}x_0 - \int_s G(\mathbf{x}|\mathbf{x}_s)\, (\partial\tilde{p}(\mathbf{x})/\partial n)_s\, \mathrm{d}\mathbf{x}_s \tag{9.22}$$

The boundary condition is expressed by the fluid momentum equation as $\partial\tilde{p}/\partial n = jk\tilde{p}(\mathbf{x}_s)/z'_n(\mathbf{x}_s)$. The source density $\tilde{q}(\mathbf{x}_0) = \tilde{Q}\delta(\mathbf{x}_0 - \mathbf{x}_q)$, where $\tilde{Q}$ is the volume source strength of a point monopole located at $\mathbf{x}_q$. Hence, Eq. (9.22) becomes

$$\tilde{p}(\mathbf{x}) = j\omega\rho_0\tilde{Q} \int_V \delta(\mathbf{x}_0 - \mathbf{x}_q) \left[\sum_N \frac{\psi_N(\mathbf{x})\,\psi_N(\mathbf{x}_0)}{\Lambda_N(k_N^2 - k^2)}\right] \mathrm{d}\mathbf{x}_0$$

$$- jk \int_s \left[\sum_N \frac{\psi_N(\mathbf{x})\,\psi_N(\mathbf{x}_s)}{\Lambda_N(k_N^2 - k^2)}\right] \frac{\tilde{p}(\mathbf{x}_s)}{z'_n(\mathbf{x}_s)}\, \mathrm{d}\mathbf{x}_s \tag{9.23}$$

We now expand $\tilde{p}(\mathbf{x})$ and $\tilde{p}(\mathbf{x}_s)$ in terms of an infinite series of rigid-wall eigenfunctions as

$$\tilde{p}(\mathbf{x}) = \sum_m \tilde{A}_m \psi_m(\mathbf{x}) \qquad \text{and} \qquad \tilde{p}(\mathbf{x}_s) = \sum_R \tilde{A}_R \psi_R(\mathbf{x}_s) \tag{9.24a,b}$$

(Students: note carefully that where a quantity is expressed as the sum of a series, different indices should be used for each substitution; if not, cross terms may be overlooked.)

Equation (9.23) becomes

$$\sum_m \tilde{A}_m \psi_m(\mathbf{x}) = j\omega\rho_0\tilde{Q} \sum_N \frac{\psi_N(\mathbf{x})\psi_N(\mathbf{x}_q)}{\Lambda_N(k_N^2 - k^2)} - jk \int_s \left[\sum_N \frac{\psi_N(\mathbf{x})\psi_N(\mathbf{x}_s)}{\Lambda_N(k_N^2 - k^2)}\right] \left[\sum_R \frac{\tilde{A}_R \psi_R(\mathbf{x}_s)}{z'_n(\mathbf{x}_s)}\right] \mathrm{d}\mathbf{x}_S \tag{9.25}$$

Multiplication by $\psi_p(\mathbf{x})$, followed by integration over the enclosure volume, yields

$$\tilde{A}_N \Lambda_N (k_N^2 - k^2) = j\omega\rho_0\tilde{Q}\,\psi_N(\mathbf{x}_q) - jk \sum_R \tilde{A}_R \int_S \left(\psi_N(\mathbf{x}_s)\psi_R(\mathbf{x}_s)/z'_n(\mathbf{x}_s)\right) \mathrm{d}\mathbf{x}_s \tag{9.26}$$

Extraction of the amplitude $\tilde{A}_N$ gives the final solution

$$\tilde{A}_N \left[\Lambda_N(k_N^2 - k^2) + jk \int_s \left(\psi_N^2(\mathbf{x}_s)/z'_n(\mathbf{x}_s)\right) \mathrm{d}\mathbf{x}_s\right]$$

$$= j\omega\rho_0\tilde{Q}\psi_N(\mathbf{x}_q) - jk \sum_{R\neq N} \tilde{A}_R \int_S \left(\psi_N(\mathbf{x}_s)\psi_R(\mathbf{x}_s)/z'_n(\mathbf{x}_s)\right) \mathrm{d}\mathbf{x}_s \tag{9.27}$$

This is the three-dimensional equivalent of Eq. (8.37). The second term on the right-hand side represents the coupling between the rigid-wall eigenfunctions that is produced by the motional response of the boundary to local pressure.

We now explicitly assume rectangular geometry and, for simplicity of expression, uniform boundary impedance. The rigid-wall eigenfunctions take the form of the space-dependent terms in Eq. (9.8). Substitution of these eigenfunctions, together with performance of the surface integration and *neglect of the cross terms* for which $R \neq N$, yields

$$\tilde{A}_N = \frac{8j\omega\rho_0\,\tilde{Q}\cos(l\pi x_q/a)\cos(m\pi y_q/b)\cos(n\pi z_q/c)}{abc[k_N^2 - k^2 + (4jk/z'_n)(1/a + 1/b + 1/c)]} \tag{9.28}$$

to which the null indices convention applies. The appearance in the denominator of the product of enclosure dimensions indicates that the pressure amplitude increases as the volume decreases.

The coupling terms under the summation sign on the right-hand side of Eq. (9.27) are generally relatively small in cases where the magnitude of the boundary impedance ratio is much greater than unity, as in a reverberant space. They are particularly small in cases where the rigid-wall model natural frequencies are well separated and at frequencies close to the natural frequency of mode N. They are only zero for pairs of rigid-wall modes that have *all* the indices of mode $N(l, m, n)$ different from those of mode $R(p, q, r)$. The neglect of cross terms is not admissible at frequencies remote from ω_N.

Equation (9.28) takes a similar form to that of the velocity frequency response of a damped simple oscillator (Appendix 5). It may be expressed more concisely as

$$\tilde{A}_N = j\omega\rho_0\tilde{Q}\beta/(\omega_N^2 - \omega^2 + jR_N - X_N) \tag{9.29}$$

where $\beta = 8\cos(l\pi x_q/a)\cos(m\pi y_q/b)\cos(n\pi z_q/c)/V$, $R_N = 4k(1/a + 1/b + 1/c)\,\mathrm{Re}\{1/z'_n\}$ and $X_N = 4k(1/a + 1/b + 1/c)I_m\{1/z'_n\}$. The subscript N is retained to indicate that the convection relating to null modal indices applies.

The equivalent loss factor $\eta_N = 4c(1/a + 1/b + 1/c)\,\mathrm{Re}\{1/z'_n\}/\omega_N$, which agrees with Eq. (9.16a), because $\delta_N = \eta_N\omega_N$. The term X_N represents the effect of the imaginary part of the boundary impedance. When negative, it represents an inertia-like response of the boundary which *increases* the 'resonance' frequency at which $|\tilde{A}_N|$ is maximum to a value greater than ω_N. When positive, it represents stiffness-like response of the boundary which *reduces* the 'resonance' frequency of maximum $|\tilde{A}_N|$ to below ω_N. The term 'resonance' is set in inverted commas because $\tilde{A}_N$ is not the amplitude of a natural mode of the enclosure; it is simply a term in the series expansion of $\tilde{p}(\mathbf{x})$.

9.9 The sound power of a point monopole in a reverberant enclosure

As we know from Section 6.7, the sound power of a source depends upon the environment in which it operates and also on the presence of any other correlated sources. The volume velocity of a point monopole in a reverberant enclosure does net work against the *resistive* component of local pressure that it induces. In principle, this pressure may be expressed as the sum of all the modal pressures at the source point. However, there exists the question of the convergence of the modal series as the distance to the source point tends to zero. The form of the free space Green's function indicates that the resistive component of pressure tends to infinity as the distance tends to zero, which suggests that the number of modes that must be taken into account increases to infinity as the distance decreases to zero. It is wise, therefore, when modelling sound radiation into an enclosure to assume a finite, but small, source region, rather than a delta function source distribution. The modal series solution then converges acceptably quickly.

We avoid this mathematical problem by restricting our attention to the sound power injected into a single rigid-wall 'mode'. The modal pressure at the source point is

$\tilde{A}_N \cos(l\pi x_q/a) \cos(m\pi y_q/b) \cos(n\pi z_q/c)$, with $\tilde{A}_N$ given by Eq. (9.29). The time-average sound power injected into a mode is

$$W = \tfrac{1}{2}\mathrm{Re}\{\tilde{p}(\mathbf{x}_q)\tilde{Q}^*\} = (|\tilde{Q}|^2\omega\rho_0\beta^2/16)[R_N/((\omega_N^2 - \omega^2 - X_N)^2 + R_N^2)] \quad (9.30)$$

When modal 'resonance' frequencies are well separated, the total harmonic source power peaks at frequencies given by $\omega^2 = \omega_N^2 - X_N$.

In the general case, Eq. (9.27) reveals coupling between the rigid-wall eigenfunctions. We must therefore not carry the isolated rigid-wall mode analysis any further. More comprehensive, rigorous analysis shows that the sound power injected by a *broadband*, random source having a uniform spectral density of source strength, *when averaged over all possible source positions*, equals that which the source would radiated into *free field*. This remarkable result is not restricted to reverberant sound fields but applies equally to the vibrational power injected into uniform, reverberant structures [9.5, 9.6]. Advantage of this result is also taken in statistical energy analysis.

9.10 Sound radiation into an enclosure by vibration of a boundary

The Green's function in the form of a series of orthogonal rigid-wall eigenfunctions may, in principle, be determined for enclosures of any geometry. We have concentrated upon a particular regular form of geometry because readers will be familiar with the trigonometric functions involved. The rigid-wall eigenfunctions of irregular enclosures may easily be determined by finite element analysis. Once found, they are very valuable because they may be employed in the analysis of acoustic coupling between the contained fluid and bounding structures, such as vehicle shells.

Sound is radiated by vibrating structures, and structures vibrate in response to sound. These two aspects of vibroacoustics are intimately related. Good radiators are good receivers. To illustrate the application of the Green's function to such systems, the problem of sound radiation by a vibrating wall panel into an enclosure of which it forms a boundary is now briefly addressed.

The wall motion is represented by a harmonic normal velocity field directed out of the fluid which has a spatial distribution represented by $\phi(\mathbf{x}_s)$:

$$v_n(\mathbf{x}_s, t) = \tilde{v}_n\phi(\mathbf{x}_s)\exp(j\omega t) \quad (9.31)$$

The K–H integral gives the pressure amplitude in the enclosure as

$$\tilde{p}(\mathbf{x}) = j\omega\rho_0\tilde{v}_n \int_S \phi(\mathbf{x}_s) \sum_N \frac{\psi_N(\mathbf{x})\psi_N(\mathbf{x}_s)}{\Lambda_N(k_N^2 - k^2 + jkr_N)} \mathrm{d}\mathbf{x}_s \quad (9.32)$$

in which $\psi_N(\mathbf{x})$ are the rigid-wall eigenfunctions and an *ad hoc* viscous modal damping term has been introduced into the Green's function to account for dissipation of sound energy by unspecified mechanisms. Its absence would lead to infinite pressures at the natural frequencies of the rigid-wall modes.

This is termed the 'uncoupled' solution because the wall motion is assumed to be inexorable (not affected by the fluid pressure). In practice, the structure is likely to be

excited by some external force and the structural response will be influenced by the response of the contained fluid. The interaction between the two dynamic systems is accounted for in a 'coupled' model formulation. The governing equations of motion of both the structure and the fluid must be solved simultaneously, subject to satisfaction of the interface boundary condition that the normal velocities of the structure and the fluid are equal.

We now assume that the system takes the form of a rectangular enclosure of which all except a single vibrating surface are rigid (Fig. 9.13). The rectangular panel is assumed to be simply supported at its edges and to vibrate harmonically in *one* of its *in vacuo* modes

$$\phi(\mathbf{x}_s) = \sin(p\pi x/a)\sin(q\pi y/b) \quad (9.33)$$

Equation (9.32) reveals that an individual panel mode drives an infinity of terms in the Green's function series. The magnitude of each coefficient of the series is determined by two factors: the difference between the panel vibration frequency $\omega = ck$ and the natural frequency ω_N of the rigid-wall mode to which the coefficient applies; and the spatial coupling coefficient formed by the integral over the surface of the panel of the product of the structural mode shape and the eigenfunction of that acoustic mode. The latter is given by

$$\int_0^a \sin(p\pi x/a)\cos(l\pi x/a)\,\mathrm{d}x \int_0^b \sin(q\pi y/b)\cos(m\pi y/b)\,\mathrm{d}y.$$

Values of low modal order integrals are presented in Fig. 9.14.

If a structure bounding a reverberant enclosure is excited by broadband forces, the interaction with the fluid is influenced by the differences between its *in vacuo* resonance frequencies and those of the rigid-wall acoustic modes, as well as by the spatial coupling coefficient introduced above. In cases where the minimum structural modal impedances, which occur at resonance and are proportional to modal damping, substantially exceed the maximum impedance presented by the fluid, which decreases with increase of sound absorption, the fluid loading effects are weak, and an 'uncoupled' analysis may be developed. This assumption has been used to good effect to deal with problems of sound radiation by vibrating structures into enclosed volumes of air, such as those in vehicle cabins and transmission of sound through building partitions which separate rooms. However, it is quite inappropriate in cases where the enclosed fluid is liquid. This is a complicated problem that is best solved by the application of variational procedures implemented by computational software packages.

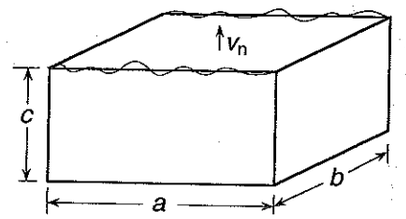

Fig. 9.13 Enclosure with vibrating wall.

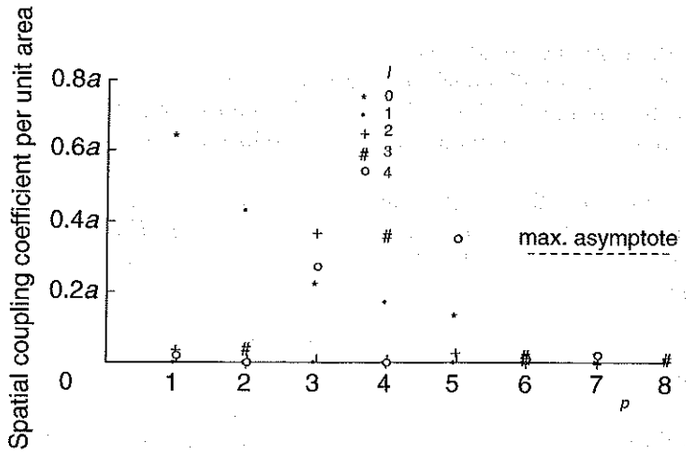

Fig. 9.14 Spatial coupling coefficient: integral over x.

9.11 Probabilistic wave field models for enclosed sound fields at high frequency

9.11.1 The modal overlap factor and response uncertainty

The asymptotic acoustic modal density of fluid in an enclosure given by Eq. (9.5) is proportional to the square of frequency. The half-power bandwidth of a mode is equal to the product of the resonance frequency and the modal loss factor (see Appendix 5). In practice, the latter tends to be rather weakly dependent on frequency. A 'modal overlap factor' may be defined to indicate the average number of modal resonance frequencies lying within the half-power bandwidth of the average mode. Its value is given by the product of the frequency, the modal-average loss factor and the asymptotic modal density; it tends to increase as the cube of frequency. This is the reason why the frequency response curve of pressure in an enclosure changes its character as frequency is increased (as evidenced by Fig. (9.2)), the individual modal peaks clustering more closely together until they can no longer be individually identified. At even higher frequencies, the logarithmic (dB) form of the curve seems to 'invert' with broad maxima being interspersed with sharp minima. The formation of the broad maxima due to the overlapping of a number of modal resonance peaks is also suggested in the diagram. However, we must not neglect to account for relative phase in this qualitative analysis, and the effect of modal overlap is more properly illustrated by the representation in terms of the complex amplitude of response as illustrated by Fig. 9.15(a).

The sensitivity of the specific form of the response curve to small variations in modal resonance frequencies is illustrated by Fig. 9.15(b), in which one is shifted by only one half power bandwidth. This typically equals $2.2/T$ Hz, where T is the reverberation time of the enclosure in that region of frequency (see Eq. (9.16(b))). Since the resonance frequencies of high-order modes are extremely sensitive to small variations in boundary geometry and impedance distribution, they can never be precisely calculated. Hence, the high-frequency response curve is *unpredictable* in detail: a probabilistic model is the only realistic alternative. A modal overlap factor of unity represents the transition between a

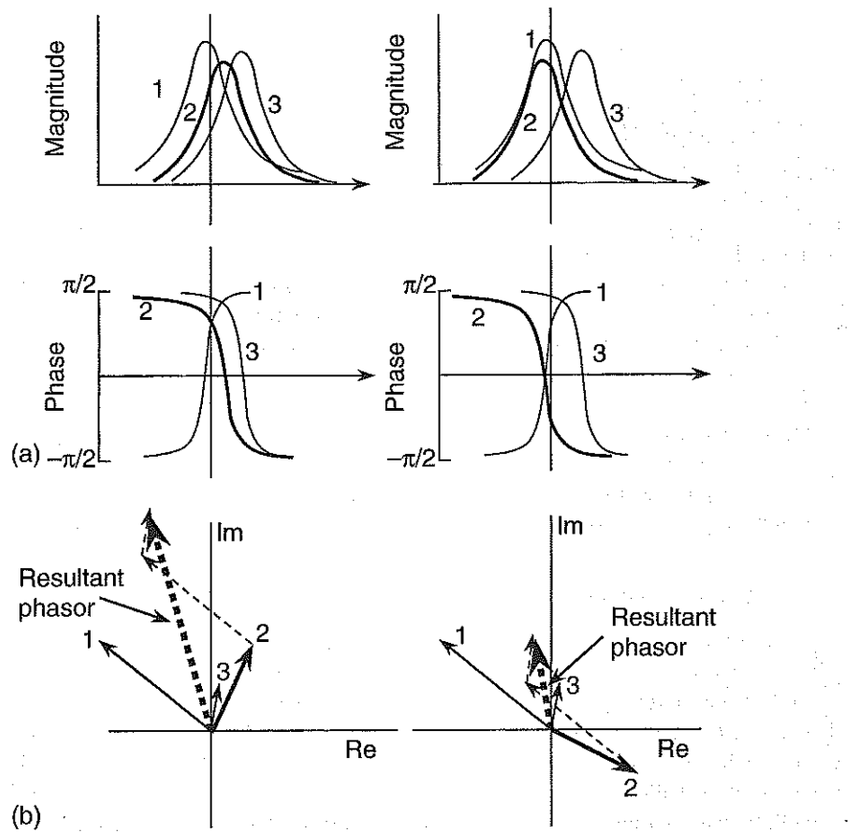

Fig. 9.15 Illustration of the sensitivity of the frequency response to a small shift of individual modal frequency.

regime of dominance of the frequency response by peaks at individual modal resonances and a regime in which the frequency response depends upon the relative amplitude and phase responses of a number of locally resonant modes. It also represents a transition between a low-frequency range in which reasonably precise deterministic estimates may be made of individual modal responses, provided that accurate information about enclosure geometry and boundary properties are available, and a high-frequency range in which only statistical estimates have any significance.

9.11.2 High-frequency sound field statistics

Research carried out during the 1950s, largely by Manfred Schroeder, showed that the transition to the probabilistic regime may be marked by that frequency at which the modal overlap factor equals three. In terms of air volume V and reverberation time T, this frequency, known as the 'Schroeder' or 'Large Room' frequency, is given by $f_s = 2000(T/V)^{1/2}$. By treating the real and imaginary parts of the complex frequency response of the pressure as independent random variables, estimates can be made of the

statistical properties of the spatial distribution of $\overline{p^2}$ and L_p at a single frequency. Above f_s, the mean square pressure is predicted to conform to a Poisson distribution, so that the probability density distribution takes the form $s(\overline{p^2}) = (1/\langle\overline{p^2}\rangle)\exp[-\overline{p^2}/\langle\overline{p^2}\rangle]$, in which $\langle\overline{p^2}\rangle$ is the space-average mean square pressure. The associated normalized standard deviation is unity. The spatial standard deviation of the logarithmic response is 5.6 dB, *independent of the physical form and properties of the enclosure*. However, the distribution is non-Gaussian leading to expected deviations from the space-average sound pressure level of +7.6 and −3.2 dB. The same figure applies to the frequency response at individual positions; Fig. 9.6(b) shows an example.

The standard deviations decrease if finite bandwidth responses are considered. The normalized standard deviation of mean square pressure in a field of bandwidth Δf Hz is given by $\sigma(\overline{p^2})/\langle\overline{p^2}\rangle \approx (6.9/T\Delta f)^{1/2}$, on condition that $T\Delta f \gg 2$ (or $\Delta f \gg \eta f$), where T is the band-average reverberation time and ηf is the average half-power bandwidth of the modes having natural frequencies in the band.

These results should be taken as a warning to those making theoretical predictions of noise levels generated in reverberant enclosures, especially where a deterministic modal model is employed. For example, air temperature changes of a few degrees Celsius are sufficient to alter harmonic response distributions by significant amounts.

9.11.3 The diffuse field model

The essential uncertainty of high-order modal parameters, together with the large populations of modes contributing to the response at any frequency under conditions of high modal overlap, require a probabilistic approach to the representation of wave fields, and to quantitative estimates of associated distributions of energy and intensity under such conditions. The previously mentioned decomposition of modal standing waves into travelling wave components suggests that a probabilistic model based on travelling waves might be feasible. The objection that pure standing waves cannot transport energy is countered by the fact that pure standing waves have been shown not to exist in tubes terminated by resistive boundaries: the natural modes are complex and capable of transporting energy. Nor do pure standing waves exist in sound-absorbent enclosures of any geometry. (It is re-emphasized that the employment of rigid-wall modes in the Green's function expansion is simply a device for simplifying the application of the K–H equation: they are not the *natural* modes of an enclosure with absorbent boundaries.)

The ideal probabilistic model, which is universally adopted to deal with the problem of describing and quantifying high-frequency sound fields in *reverberant* enclosures, is that of the diffuse field. The central concept is that of a sound field consisting of a very large set of *statistically unrelated* (*uncorrelated*) elemental plane waves of which the propagation direction is random with a uniform probability distribution. The assumption of zero correlation affords vital simplification, because it excludes interference between different elemental waves and allows mean square pressures and intensities associated with each wave to be summed.

This conceptual 'leap' from a sound field comprising a large number of modes that are, as individuals, fully correlated distributions of field quantities, to a completely uncorrelated set of travelling waves, is not easy to grasp (or even accept). In fact, it conceals many problematic theoretical aspects that cannot be explored here. However, appeal to the image source model introduced in Section 9.4 may be found useful in

clarifying the issue. Let us imagine that the physical point source has a broadband random source strength with a uniform spectrum: so too do the images. A feature of broadband random signals is that they have a short 'memory'; the correlation between a signal and a time-shifted version of itself is negligible for a time shift much greater than the inverse of frequency bandwidth. Consequently, signals from broadband random images situated at different distances from the observation point in the enclosure lose correlation as that distance increases. In a highly reverberant enclosure, image strength decreases slowly with distance from the observation point, and a large number of them are influential. The larger the enclosure, the more separated are the images, and the further they are away, the more plane become their wavefronts as they traverse the enclosure. So, the field may be considered to consist of the superposition of many travelling waves that become increasingly uncorrelated as the bandwidth of the source and the size of the enclosure increase. Spatial isotropy is favoured by enclosures whose principal dimensions are similar, and in which the average absorption coefficient is low and fairly uniform over the complete boundary, so that the images are reasonably uniformly distributed in virtual space and the image strength distributions are similar in all radial directions.

If the enclosure boundaries do not reflect faithfully (specularly) but, at each successive reflection, progressively fragment the incident wavefronts and scatter the incident sound energy into many directions, one could imagine that the time delays between the arrival of the multiply fragmented elements of wavefront at an observation point become essentially random. This behaviour further promotes lack of correlation between the associated waves as they travel through the enclosure. The presence of scattering objects within the enclosure will have a similar effect. Correlation can be even further reduced by exciting the enclosure by a number of uncorrelated sources located at different positions.

This qualitative exposition suggests that the conditions favouring the establishment of a quasi-diffuse field are as follows:

1. A large, highly reverberant enclosure having similar principal dimensions;
2. Similar average absorption coefficients on each section of the boundary;
3. Strongly scattering boundaries and/or objects within the enclosure;
4. More than one broadband source.

It is obvious from the image model that *pure tone* sources cannot generate an ideal diffuse field in the sense we have defined above. The source bandwidth necessary to generate a quasi-diffuse field decreases with increase of enclosure volume.

The apparently plausible diffuse model appears at first sight to have a fatal flaw. If uncorrelated plane waves of *equal* mean square pressure, and therefore equal intensity, propagate in all directions with equal probability, the field is spatially isotropic and the net intensity is everywhere *zero*. It would therefore appear that sound energy cannot flow from a source to the absorbent boundaries. This would indeed be the case if the direct field of the source were neglected. We know from Chapter 5 that the integral over any enveloping surface of the normal component of intensity equals the total sound power of steady sources operating within the enveloped volume. The intensity at any point on a surface enveloping a point source in an enclosure equals the sum of the intensities of the direct field of the source and of the reverberant field, *if the two field components are uncorrelated.* A reverberant field must therefore make a negligible contribution to the integral over any surface enveloping the source(s), whatever its degree of topological

complexity. The ideal diffuse field certainly satisfies this requirement; but this alone is not sufficient to explain how it can be responsible for contributing to the dissipation of the source power. It is possible for uncorrelated plane waves to transport energy in all directions towards the enclosure boundaries without invalidating the condition of zero net intensity. The process of boundary absorption can be likened to a distribution of negative sources (known as 'sinks') that operate *outside* any surface enveloping the source. According to Section 5.8, they have no influence on the surface integral of normal intensity. The weakened reflected waves pass through the enveloping surface but have no net effect on the surface integral.

It might be helpful to reconsider this scenario in the case of an impulsive source, as illustrated by Fig. 9.16. The initial (direct field) wavefront passes out through an enveloping surface separating the source from the boundary. The transmitted energy is registered. A proportion of this energy is absorbed upon first encounter with the boundary. The weakened reflected wavefronts pass *into* and *out of* the surface, producing no net energy exchange. They are again reflected by the boundary, which both weakens and redirects them. This process continues until all the energy is dissipated. Only the energy carried by the direct field wavefront is registered; but this is dissipated gradually by reflections of the 'reverberant' field. In steady state, these processes operate continuously, and a large enough assembly of coexisting reflected waves travelling in many directions may easily be imagined to produce zero net intensity, yet be responsible for dissipating the major part of the energy radiated by the source.

This discussion suggests a simple test for the degree of diffuseness of a reverberant sound field. The intensity directivity of a source in free field will persist at all distances if the reverberant field is ideally diffuse. The dominance of the direct field intensity over a diffuse field component of much higher energy density is supported by the experimental observation that a broadband source in a reverberant room may be easily located by the null indication of an intensity measurement system at almost all points within the room. (Note: the intensity null lies on an axis perpendicular to the intensity vector and is much more sensitive to probe orientation than the intensity maximum.)

The intensity distribution over a surface enclosing a steady source in an enclosure where the absorption is concentrated on one region of the surface is illustrated qualitatively in Fig. 9.17. The field is clearly not diffuse. The figure suggests that the

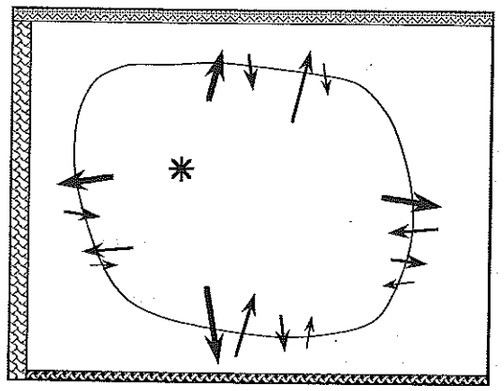

Fig. 9.16 Impulse intensity sequence.

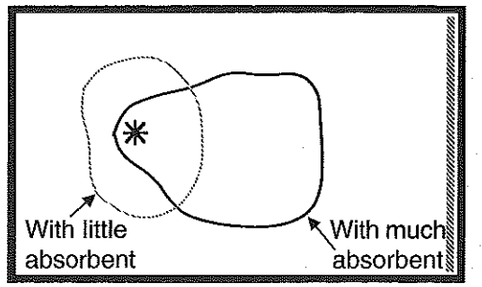

Fig. 9.17 Radial intensity distribution around a source in an enclosure having one absorbent wall.

presence of one highly absorbent region creates a 'diffusion deficit' in the sound incident upon *other* surfaces. However, it does not itself suffer such a serious deficit (under steady state conditions). This physical situation arises in relation to International Standard ISO 354 for the determination of diffuse field sound absorption coefficient by measurements of reverberation time in a reverberation chamber fitted with an absorbent sample on *one* boundary. The estimate of sound absorption coefficient is based upon an assumption of a diffuse field to relate absorbed power to reverberation time (see the following section). The standard does recognize the problem of lack of diffusion and allows the installation of diffusing elements suspended within the volume. Their presence scatters incident sound. The direct sound from the source is thus scattered before reaching the test specimen and the reverberant energy is 'rediffused' after each reflection.

The fact that the sound power of a broadband source in a reverberant enclosure is very similar to its free field power, except when placed close to boundary, also throws some light on the characteristics of reverberant fields in enclosures. It was shown in Section 6.7 that the sound power of a source is altered by the incidence upon it of sound generated by another *correlated* source. The incidence of many uncorrelated waves incident upon a source far from a boundary has no effect on its sound power. But, with a source close to a boundary, the first-order image (or the reflected wave which it represents) is too close to be uncorrelated, and the source sound power is altered. The form of effect is seen in the 'in-phase' curve of Fig. 6.20, although the decay of the effect with distance is more rapid with broadband sources.

The incident and reflected wave components of a reverberant field are also mutually correlated close to a boundary because, together, they have to satisfy the local boundary condition. As a result, the space-average mean square *boundary* pressure in a broadband reverberant field is twice that in the central field region in which boundary correlation effects are absent. The corollary is that the spatial-average sound pressure level generated by a *small* Category 1 source is increased by 3 dB on close approach to a highly reflective boundary: so too is the sound power. This is a manifestation of acoustic reciprocity. The theoretical increases are 6 dB near an edge and 9 dB near a corner. Engineers should note that these increases are not generally achieved by real, spatially extended noise sources, partly because the various radiating regions are necessarily located at different distances from the boundary, and partly because vibrating bodies are not pure Category 1 sources.

9.12 Applications of the diffuse field model

9.12.1 Steady state diffuse field energy, intensity and enclosure absorption

Having discussed at length the assumptions and attributes of the ideal diffuse field, we now turn to its quantitative implications. An approximation to a diffuse field may be produced in free field at the centre of a spherical surface on which uncorrelated, stationary, random monopoles of equal mean square source strength are uniformly and densely distributed, as illustrated by Fig. 9.18. The monopole source strength is defined as $\rho_0\dot{Q}(t)$ *per unit area* of spherical surface. Because the associated sound fields are uncorrelated, the mean square pressure at the centre of the sphere is, from Eq. (6.23),

$$\overline{p^2} = (\rho_0/4\pi R)^2 4\pi R^2 \overline{\dot{Q}^2} = \rho_0^2 \overline{\dot{Q}^2}/4\pi \tag{9.34}$$

which is independent of the radius of the sphere R.

The time-average normal intensity produced on a plane of symmetry by the monopoles located on *one side* of the plane in a ring of radius $R \sin\phi$, which subtends angle $d\phi$ at the centre, is

$$\overline{I_n}(\phi) = \overline{\dot{Q}^2}(2\pi R^2 \sin\phi\, d\phi)(\rho_0/4\pi R)^2 \cos\phi/\rho_0 c \tag{9.35}$$

The total intensity generated by the sources on one side is

$$\overline{I_n} = \overline{\dot{Q}^2}(\rho_0/16\pi c)\int_0^{\pi/2} \sin 2\phi\, d\phi = \overline{\dot{Q}^2}\rho_0/16\pi c \tag{9.36}$$

Hence, from Eq. (9.34), the 'one-sided intensity' is

$$\overline{I_n} = \overline{p^2}/4\rho_0 c \tag{9.37}$$

where, in the general physical case, $\overline{p^2}$ represents the space-average mean square pressure in the diffuse field *remote from boundaries*. If the plane concerned were rigid, the mean square pressure on the surface would equal twice that in Eq. (9.34) because only half the sources would contribute, but pressure doubling would occur at the surface. Of course, according to this ideal model, the total (two-sided) intensity in the diffuse field is zero.

Consequently, the relation between the time-average incident power per unit area of boundary and the time-average energy density under steady state, diffuse field, conditions is

$$\overline{I_n} = \overline{p^2}/4\rho_0 c = c\bar{\varepsilon}/4 \tag{9.38}$$

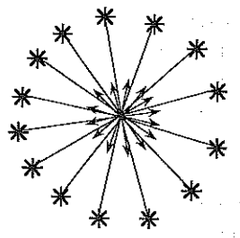

Fig. 9.18 Spherical array of uncorrelated monopole sources, which generates the ideal diffuse field at the centre.

The total time-average energy stored in the enclosed field is

$$\overline{E} = \overline{p^2}V/\rho_0 c^2 \tag{9.39}$$

where V is the enclosure volume. (In real, quasi-diffuse sound fields, neither $\bar{\varepsilon}$ nor $\overline{p^2}$ are spatially uniform. They are therefore usually replaced by the space-average values $\langle\bar{\varepsilon}\rangle$ and $\langle\overline{p^2}\rangle$.) The total time-average rate of absorption of diffuse sound energy by the enclosure boundary is

$$\overline{W}_{abs} = \overline{I_n}\sum_i S_i\alpha_{di} = \overline{I_n}\langle\alpha_d\rangle_i\sum_i S_i = (\overline{p^2}/4\rho_0 c)\langle\alpha_d\rangle_i\sum S_i \tag{9.40}$$

where α_{di} is the diffuse field absorption coefficient of boundary area S_i and $\langle\alpha_d\rangle_i$ is the weighted arithmetic average diffuse incidence absorption coefficient, conventionally denoted by $\bar{\alpha}$, and defined by

$$\bar{\alpha} = \sum_i (S_i\alpha_{di})/\sum_i S_i = \sum_i (S_i\alpha_{di})/S \tag{9.41}$$

The quantity $S\bar{\alpha} = A$ (unit: m^2) is known as the 'absorption' of the enclosure.

9.12.2 Reverberation time

We now consider the rate of change of sound energy stored in a *reverberant* enclosure during the initial part of the energy decay process following impulsive excitation, or the cessation of a continuous source. On the basis of the argument that the proportional loss of energy during the average period of oscillation of the field quantities is very small, it is reasonable to assume quasi-steady conditions, in which averages taken over intervals of the order of one hundred times that period are meaningful. We also assume that the diffuse field model holds good.

The rate of loss of diffuse field energy, given by Eq. (9.40), is proportional to the total field energy, given by Eq. (9.39). Hence the energy decays exponentially according to

$$E(t) = E(0)\exp(-\delta t) \tag{9.42}$$

where $\delta = Ac/4V$. The corresponding reverberation time $(E(T)/E(0)) = 10^{-6})$ is given by

$$T = 13.8/\delta \tag{9.43}$$

In air at 20°C,

$$T = 0.16V/A \tag{9.44}$$

This formula was derived in the early twentieth century by W. C. Sabine. A later, more refined model suggested that A should be replaced by $S\bar{\alpha}/(1-\bar{\alpha})$. Unlike Sabine's equation, this form predicts zero reverberation time in an anechoic chamber. However, the assumptions underlying the derivation of both equations invalidate their use in many cases of practical interest, and it is necessary to apply a geometric acoustic analysis, as explained in the following section.

Equation (9.44) forms the basis of the most common method of estimating experimentally the sound absorption of an enclosure. The sound field is excited either by a continuous broadband noise source that is suddenly terminated, or by an impulsive source such as a starting pistol. The initial rate of decay of the short-term-average

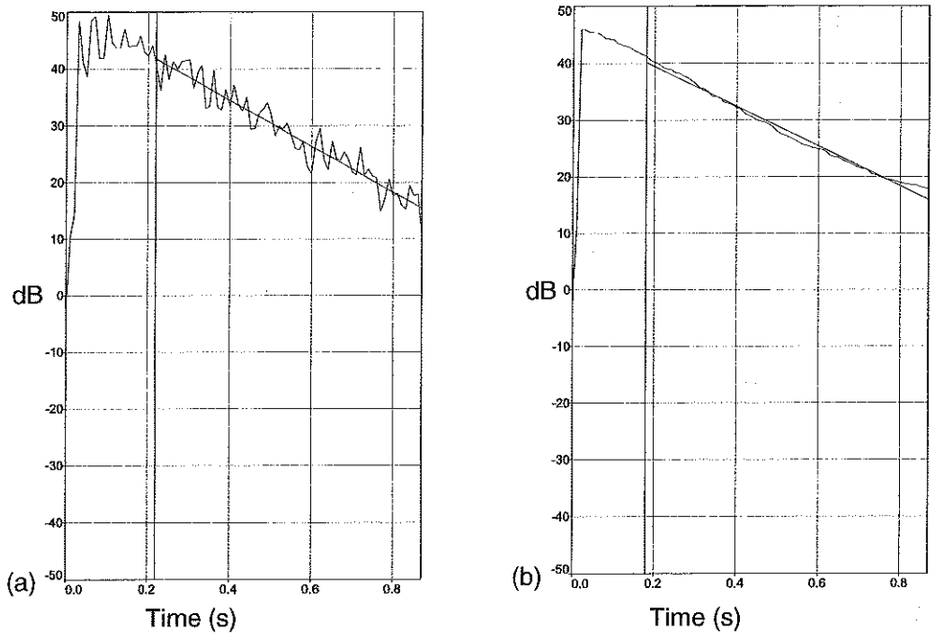

Fig. 9.19 (a) Conventional reverberation decay curve (1.25 kHz, T = 1.48 s). (b) Schroeder integrated impulse curve (1.25 kHz, T = 1.71 s). Courtesy of J. Shelton, AcSoft Ltd.

squared pressure at a number of source and microphone positions is measured. A typical curve of decay following cessation of a band-limited, random excitation is shown in Fig. 9.19(a). This curve will not repeat precisely because the initial conditions are random. This randomness, together with the associated need to repeat the measurement many times at one point to reduce the random error, may be removed by applying Schroeder's 'integrated impulse' technique. The band-limited impulse response of the enclosure is determined by means of an FFT analyser. The bandwidth must be sufficiently large to ensure that the filter impulse response decays much more rapidly than that of the enclosure. The impulse response is squared, and integrated over *reversed* time, starting at a time by which the impulse response has decayed to a negligible value. This process effectively provides the ensemble average of an infinity of curves obtained by the decay method and therefore eliminates random error, as illustrated by Fig. 9.19(b). Because no physical reverberant fields are truly diffuse, it is necessary to obtain an ensemble-average estimate of decay rates over a range of source positions and orientations, and receiver positions.

It must be understood that Eqs (9.40) and (9.44) are only valid under a range of very restrictive conditions. In cases where they do not obtain, for example within fully trimmed vehicle interiors, it is preferable to employ an alternative, steady state relation presented in the following section. For example, at frequencies higher than about 500 Hz, the sound field in a fully trimmed car is not reverberant, and the above relations are entirely irrelevant.

9.12.3 Steady state source sound power and reverberant field energy

The field that arises from multiple reflections by the enclosure boundary of the sound emitted by a source is conventionally distinguished from the direct (free) field of the source by calling it the 'reverberant' field. It may not be diffuse, but if assumed to be so, the following analysis relates the sound power of a steady source to the time- and space-averaged mean square sound pressure in the reverberant field.

The time-average sound power radiated by any steady source in a reverberant enclosure equals the time-average rate of absorption of sound energy by the boundaries of the enclosure (plus that of any objects present within the enclosure, which we shall not consider here). If we assume that all the power is injected into the reverberant field, Eqs (9.40) and (9.41) give the space-average mean square pressure in the reverberant field as

$$\langle \overline{p_r^2} \rangle = 4\rho_0 c \overline{W}/A \tag{9.45}$$

where $\overline{W}$ is the time-average source power. In terms of the reverberation time this becomes

$$\langle \overline{p_r^2} \rangle = 25\rho_0 c T \overline{W}/V \tag{9.46}$$

If, instead, we assume that the sound power injected into the reverberant field is that which is not absorbed by the incidence of the *direct* field on the boundary, we must correct Eqs (9.45) and (9.46). The correction is problematic because the direct field is not plane and has no unique angle of incidence at the boundary. The best we can do is to assume that many angles are involved and therefore assume that the sound power injected into the reverberant field is $\overline{W}(1 - \bar{\alpha})$, which alters Eq. (9.45) to

$$\langle \overline{p_r^2} \rangle = 4\rho_0 c \overline{W}(1 - \bar{\alpha})/A \tag{9.47}$$

Since the diffuse field relations we have used are only appropriate to enclosures in which $\bar{\alpha} \ll 1$, the correction is small. A hydraulic analogy of the balance of radiated and absorbed sound power is presented in Fig. 9.20.

A simplistic idealization of the spatial distribution of sound pressure level in a reverberant enclosure is presented in Fig. 9.21, in which the direct and reverberant fields are assumed to be uncorrelated. The total mean square pressure at distance r from the source centre is given by

$$\overline{p_r^2(\Omega)} = \rho_0 c\, \overline{W}[D(\Omega)/4\pi r^2 + 4(1 - \bar{\alpha})/A] \tag{9.48}$$

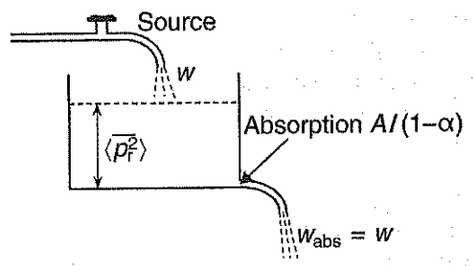

Fig. 9.20 Hydraulic analogy of energy balance in a reverberant enclosure driven by a source.

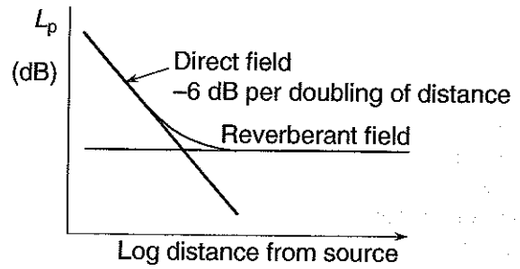

Fig. 9.21 Simplistic model of sound level distribution in a reverberant enclosure driven by a source.

in which $D(\Omega)$ is a source directivity factor. The distance at which the two components of mean square pressure are equal is known as the 'reverberation radius', given by

$$r_r = [AD(\Omega)/16\pi(1-\bar{\alpha})]^{1/2} \tag{9.49}$$

It is proportional to the square root of the absorption of the enclosure.

Example: One of the ISVR acoustics teaching labs has a volume of about 280 m^3, a surface area of about 290 m^2 and an experimentally estimated absorption of about 40 m^2, which is rather independent of frequency. The reverberation radius of an omnidirectional source is therefore just under 1 m.

This simple distribution of sound pressure level distribution is only well approximated in empty, highly reverberant, rooms having rather similar principal dimensions excited by broadband sources. It is rarely observed in practice and should never be used to predict sound pressure level distributions in furnished rooms of any form. Even in very large, empty, reverberant industrial halls, the scattering effect of the walls and roof is sufficient to cause the steady state sound pressure level to fall continuously with distance from a broadband source. In spaces containing large scattering objects, such as industrial machines, the L_p versus distance curve takes a totally different form from that in Fig. 9.21, as shown by Fig. 9.22.

The effective absorption of an enclosure may be obtained by using the relation between space-average mean square pressure and injected sound power (Eq. (9.45)). In order conveniently to measure injected power, a compression driver is connected to a short length of uniform tube that has its lowest cut-off frequency above the highest frequency of interest. The tube is connected to an acoustic horn of suitable size for the application; it may be dispensed with if necessary. Two or more phase-matched microphones are set into the side of the tube. The imaginary part of the cross spectrum gives the transmitted intensity (see Section 5.7), which, when multiplied by the cross-sectional area of the tube, gives sound power. (Microphone pair reversal, together with arithmetic averaging of the two intensity estimates, removes the need for very precisely matched microphones and also removes bias error.) Measurement of the mean square pressure at a number of points in the enclosure not close to the horn mouth allows the absorption to be estimated. Because steady state excitation is employed, the conditions more closely resemble the operational situation, and uncertainties concerning the estimate of energy decay rate and its relation to steady state absorption are obviated.

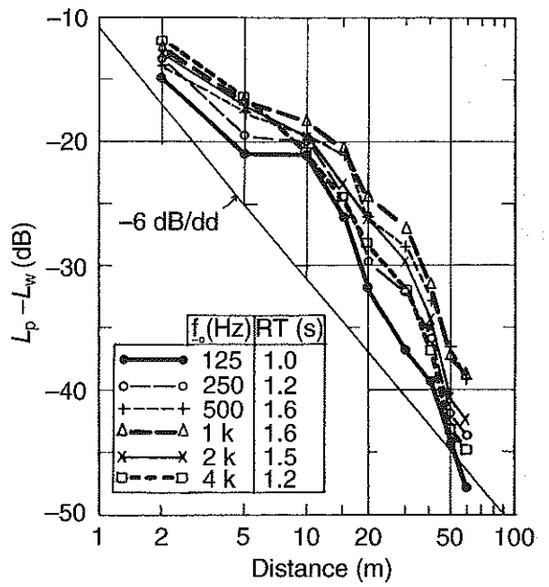

Fig. 9.22 Typical sound propagation curves in a fitted factory. Reprinted from *Applied Acoustics*, volume **16**, M. Hodgson, 'Measurement of the influence of fittings and roof pitch on the sound fields in panel-roof factories', pp. 369–392, copyright (1983), with permission from Elsevier Science.

9.13 A brief introduction to geometric (ray) acoustics

It has become clear from the previous section that the ideal diffuse field model is not well suited to the representation of sound fields in enclosed spaces that are not highly reverberant, that have one or two principal dimensions much greater then other(s), that have highly non-uniform distributions of sound absorption over the boundaries, and that contain large numbers of scattering objects which, by back scattering, impede the transmission of sound energy between different regions.

The wave acoustics model is essential in cases where the principal dimensions of the enclosure are of the same order as the acoustic wavelength. This is because wave interference dominates the sound field in the form of modes, resonances and diffraction. In other cases, where the acoustic wavelength is much smaller than the dimensions of an enclosure, interference effects are still observable if the source emits a single frequency but, because of the great density of modal frequencies, they largely disappear when the bandwidth of a source emits even a rather narrow band of frequencies.

The acoustic behaviour of enclosed spaces such as offices, industrial workshops, airport lounges, railway stations and auditoria, which are occupied by many persons and many inanimate objects, is of concern to engineers in relation to speech communication and/or noise control. The frequency range of concern typically ranges from 50 to 5000 Hz. Over much of this range, the topologies of the enclosure boundaries and contents are irregular on the scale of an acoustic wavelength. In addition, the impedances of the various surfaces often vary widely over distances comparable with a wavelength. The combined effect is to scatter incident sound energy into many different directions.

Since it is obviously impossible to model this process on the basis of the wave equation, various forms of geometric ray model have been developed for implementation by computer. Sound energy is assumed to be carried by discrete rays and interference is neglected. A source is assumed to emit continuous rays in a large number of uniformly spaced radial directions, the angular distribution of intensity being specified according to source directivity. The energy propagating in a ray is conserved during free propagation (sometimes with air absorption imposed). The divergence of the rays automatically accounts for spherical spreading of the energy, so that the intensity decreases as the square of the distance travelled.

When a ray strikes an enclosure boundary, the energy is partially reflected and partially absorbed, usually on the basis of the assumption of the relevant diffuse field absorption coefficient. Calculations are normally made at octave band centre frequencies, account being taken of frequency dependence of absorption coefficients. Some models account for the dependence of absorption coefficient on the incidence angle, but in a highly reverberant space where many rays strike a given surface at different angles, this refinement makes little difference to the result. The reflections are normally assumed to be specular so that a discrete ray emerges from the encounter (see the discussion of reflection in Chapter 12). Although research indicates that most surfaces in industrial workshops scatter a proportion of incident sound energy into non-specular directions, it is not at present practicable to generate many rays upon each reflection because the number of rays that would have to be followed would escalate out of manageable proportions.

When a ray strikes a 'fitting' element (discrete object), such as a machine in a workshop, a proportion of the energy is assumed to be absorbed, the rest being randomly scattered. Each scattering event is modelled as a virtual omnidirectional source. The modelling of the scattering effect of fittings is crucial to the accuracy of the estimation of sound pressure levels in spaces containing many discrete scatterers, but current models are not fully satisfactory in this respect, not least because it is difficult to estimate the scattering effectiveness of fittings of disparate size, shape and material.

Receiver volumes are distributed throughout the region in which it is wished to determine the sound pressure level. For the estimate of steady state levels, the energy of each ray passing through a volume is accumulated. Rays are extinguished once they have lost most of their energy: the extinction criterion varies from program to program. In order to estimate reverberant decay behaviour the time sequence of energy 'strikes' is recorded.

A typical example of the spatial variation of steady state sound pressure level generated by a single source in a fitted factory space is presented in Fig. 9.22. The curve takes a completely different form from that of Fig. 9.21.

Recent developments in this modelling procedure include the provision of simple models of barrier diffraction and some degree of phase representation to account for interference effects at low frequencies, although the previously mentioned chaotic nature of enclosed sound fields makes it difficult to accept the reliability of such representation.

A combination of image, ray and statistical models is employed in software for the 'auralization' of auditoria by means of which projected designs can be aurally sampled, and the effect of design changes assessed [9.3]. A recent development, which is computationally very efficient, models sound propagation through a network of 'digital waveguides' [9.7]. Its effectiveness remains to be fully evaluated.

Questions

9.1 A small lecture room measuring 6 m × 10 m × 3 m has plastered concrete walls. The seating covers 80% of the floor area. The empty reverberation time in the 500 Hz 1/3 octave band is 1.3 s. The estimated diffuse field absorption coefficient of the walls and uncovered floor in this band is 0.05. Estimate the absorption coefficient of the seating area in the 500 Hz band.

9.2 The sound power of a source in the 500 Hz 1/3 octave band is 10^{-3} W. It is placed in a room having a volume of 150 m^3 and reverberation time in this band of 1.2 s. Estimate the space-average reverberant mean square pressure and the corresponding sound pressure level.

9.3 A small enclosure has two acoustic mode natural frequencies of 121 Hz and 132 Hz in the 125 Hz 1/3 octave band. The corresponding modal loss factors are 10^{-2} and 1.6×10^{-2}, respectively. Calculate the individual modal reverberation times. Use a computer to display the time history of the pressure during free decay resulting from the superposition of the modal pressures at a position where the initial modal pressure amplitudes and phases are equal. What does the result tell you about attempts to measure reverberation time in narrow bands in small enclosures at low frequency?

9.4 Construct an image set for a rigid-walled, rectangular room of dimensions 10 m × 6 m × 3 m with a 100 Hz harmonic point monopole situated at a point of your choice. The source is suddenly switched on at a time of zero volume acceleration. Synthesize the complex pressure amplitude at another point of your choice by means of sequential addition of the sound pressures generated at the receiver point. The sequence is determined by the relative distances of the images from the receiver point. Output the real pressure amplitude after each addition. Don't forget to include the direct field. Observe the evolution of the pressure amplitude as the largest image distance increases. Does the sum converge? Compare the results with the receiver point at distances of 0.3 and 6 m from the source. Also, select a frequency that corresponds to one of the rigid-wall mode natural frequencies. What do you learn from these studies? How could you modify your model to ensure convergence?

9.5 A dipole source consisting of two closely spaced harmonic point monopoles of opposite sign is substituted for the monopole in the previous question. Select a suitable separation distance and exploit the principle of superposition. How do the results differ from those with monopole excitation in qualitative terms? Can you offer physical reasons for the differences?

9.6 What is the average absorption coefficient of the ISVR room described in Section 9.12.3?